International Journal of Nanomedicine

Dovepress
open access to scientific and medical research

Open Access Full Text Article

ORIGINAL RESEARCH

Combined Verapamil-Polydopamine Nanoformulation Inhibits Adhesion Formation in Achilles Tendon Injury Using Rat Model

Shaoyan Li[1,2,*], Fengyan Gong[1,2], Zekun Zhou[1,2,*], Xu Gong[1,2]

[1]Department of Hand and Podiatric Surgery, Orthopedics Center, The First Hospital of Jilin University, Changchun, 130021, People's Republic of China; [2]Jilin Province Key Laboratory on Tissue Repair, Reconstruction and Regeneration, The First Hospital of Jilin University, Changchun, 130021, People's Republic of China

*These authors contributed equally to this work

Correspondence: Xu Gong, Department of Hand and Podiatric Surgery, Orthopedics center, The First Hospital of Jilin University, Changchun, 130021, People's Republic of China, Tel +86-13944099151, Email gongxu@jlu.edu.cn

Introduction: Topical verapamil has been demonstrated to reduce the fibroproliferative scar. Therefore, it was hypothesized that topical verapamil could reduce adhesion formation after tendon repair. The current study aimed to examine the effects of verapamil-loaded polydopamine nanoparticles (VP-PDA NPs) on the adhesion formation of Achilles tendon laceration and repair in a rat model.

Methods: We randomly assigned 72 male Sprague-Dawley rats to the control, the PDA NPs, and the VP-PDA NPs groups (n = 24 per group). The quality of tendon healing was evaluated by the maximal tensile strength four and six weeks after surgery. The degree of tendon adhesion was scored on days 4, 15, 29, and 43 after surgery. The expressions of transforming growth factor-beta 1 (TGF-β1), vimentin, α-smooth muscle actin (α-SMA), and collagens type I and III were detected through Western blotting or immunohistochemistry at four weeks after surgery.

Results: In vitro release tests revealed that 61.3% of verapamil was released from VP-PDA NPs in four weeks. There was a significant increase in average failure to load in the VP-PDA NPs group (89.27 ± 5.09 N) compared with the PDA NPs group (65.52 ± 2.04 N) (p = 0.003) and the control group (74.52 ± 4.24 N) (p = 0.029). Adhesion scores were significantly reduced in the VP-PDA NPs group at six weeks (3.175 ± 0.08) and four weeks (3.35 ± 0.25) compared with the other groups. Moreover, VP-PDA NPs significantly reduced the expression of vimentin, α-SMA, TGF-β1, and collagens type I and III.

Conclusion: These data suggest that VP-PDA NPs reduced adhesion formation and enhanced tendon healing during rat tendon injury. Since topical verapamil has been used in clinics without side effects, VP-PDA NPs would have direct translation implications. However, its anti-adhesive effects on intrasynovial tendon injury must be examined.

Keywords: tendon injury, adhesion formation, verapamil, nanoparticle

Introduction

Tendon injury is quite common in daily living without ideal therapeutic outcomes.[1–4] The major cause affecting tendon repair efficacy is adhesion formation between the tendon surface and surrounding tissue, leading to loss of tendon gliding function.[1–4] Clinically, early active or passive controlled mobilization after tendon repair is the only effective modality for decreasing adhesion formation. Nonetheless, about 30% to 40% of patients with tendon injuries end up with tendon adhesion.[1–4] Over the past several decades, various modalities have been investigated for enhancing tendon healing and reducing adhesion formation.[5–21] However, optimal regimens have not been determined.[1–4]

Verapamil, a calcium channel blocker, effectively reduces hypertrophic scars through the topical application without adverse effects.[22–28] As depicted by the in vitro experiment, calcium channel blockers decrease collagen deposition by inhibiting the expression of collagen genes and increasing the proteolytic activity of collagenase type III.[29] As adhesion

Received: 14 June 2022
Accepted: 23 December 2022
Published: 6 January 2023

formation after tendon repair is a scar between the injured tendon and surrounding tissue,[30] topical application of verapamil could decrease adhesion formation after tendon repair.

Topical long-acting sustained release of verapamil for reducing adhesion formation is favorable for tendon injury and repair. This is because it avoids the side effects of systemic hypotension and maximizes the anti-adhesive effects. In this study, we examined the effects of a novel verapamil formulation, viz., verapamil-loaded polydopamine nanoparticles (VP-PDA NPs), on adhesion formation of Achilles tendon laceration and repair in a rat model.

Materials and Methods

Preparation of Polydopamine Nanoparticles and Verapamil-Loaded Polydopamine Nanoparticles

Polydopamine nanoparticles (PDA NPs) were synthesized by adding 0.6 g dopamine hydrochloride (99.9%; Sigma, Cat# H8502-25G, St. Louis, USA) into a solution comprising 85 mL Tris buffer solution (pH 8.50; Macklin, Cat# T819511-25g, Shanghai, China) and 15 mL ethanol (99.7%; Sinopharm Chemical Reagent co., Ltd., Cat# 10009297, Beijing, China). The mixture was centrifuged at 8800 r/min for 10 min to obtain PDA NPs after stirring for 24 h at room temperature. VP-PDA NPs were synthesized by mixing equal volumes of 2 mg/mL PDA NPs solution with 2 mg/mL verapamil hydrochloride (> 98.0%; Shanghai Yuanye Bio-technology Co., Ltd., Cat# B27033, Shanghai, China). The mixture was centrifuged at 8800 r/min for 10 min after stirring for 24 h at room temperature to obtain VP-PDA NPs.

Characterization of Polydopamine Nanoparticles and Verapamil-Loaded Polydopamine Nanoparticles

The morphology and size of PDA and VP-PDA NPs were detected using transmission electron microscopy (TEM) (JEM-2100F, Jeol, Japan). Verapamil loading in VP-PDA NPs was verified through Fourier transform infrared spectrometer (FTIR) (Vertex 80V, Bruker, Germany). The standard curve method was used to determine the drug-loading rate and encapsulation efficiency of VP-PDA NPs. The ultraviolet (UV) absorption spectrum of verapamil hydrochloride solution was first tested using a UV-Vis spectrophotometer (Shimadzu UV-2600, Japan) at different concentrations (0.025, 0.050, 0.075, and 0.100 mg/mL). Then, a standard curve of UV absorbance value against the solution concentration was fitted based on their absorbance value at the maximum absorption wavelength. Depending on the standard curve, the concentration of unloaded verapamil in the supernatant after drug loading was obtained through the UV absorption value of the supernatant. We calculated the drug-loading rate and encapsulation efficiency of VP-PDA NPs using the following formulas.

$$R_l = \frac{C_{iv} - C_{sv}}{C_{iv} - C_{sv} + C_p}$$

$$R_e = \frac{C_{iv} - C_{sv}}{C_{iv}}$$

R_l: drug-loading rate;
R_e: encapsulation efficiency;
C_{iv}: initial concentration of verapamil hydrochloride;
C_{sv}: verapamil hydrochloride concentration in the supernatant;
C_p: initial concentration of polydopamine nanoparticle

In vitro Verapamil Release of Verapamil-Loaded Polydopamine Nanoparticles

VP-PDA NPs were dissolved in PBS solution (pH 7.2–7.4; Solarbio, China). A 2 mL aliquot from the solution was taken every two days for four weeks and centrifuged at 18,000 r/min for 10 min. The amount of verapamil was obtained by determining the concentration of verapamil hydrochloride in the supernatant based on the standard curve.

Study Design

Seventy-two male Sprague-Dawley rats (7 weeks of age; body weight: 260 ± 20 g) were randomly assigned to control, PDA NPs, and VP-PDA NPs (n = 24 per group) groups. The animals were treated humanely based on the guidelines in the Guide for the Care and Use of Laboratory Animals published by the National Institutes of Health (USA). Moreover, the rats were housed in individual cages at room temperature (23–25 °C) using ad libitum food pellets and water. All the experiments were conducted under general anesthesia through 4% isoflurane. The experimental protocol was approved by the Institutional Review Board of the Jilin University First Hospital (Approval No. 20210064).

Surgical Procedure

A 2 cm skin incision was made longitudinally along the Achilles tendon in the unilateral hindlimb. After the accessory tendon was excised, the Achilles tendon was exposed and entirely transected at 0.75 cm proximal to its insertion. The transected tendons were repaired using a modified Kessler method by a 6–0 nylon suture (Round needle 3/8, 2.5 × 8; Yuankang Medical, Yangzhou, China). After completing tendon repair, 4 mg PDA NPs or 5 mg VP-PDA NPs (3.865 mg PDA NPs + 1.135 mg verapamil as described below) were administered across the repaired tendons. The skin was closed interruptedly by a 4–0 suture. After surgery, the rats could mobilize freely in an individual cage without external immobilization. At the designated time, the rats were euthanized with an excessive anesthetic.

Biomechanical Testing

Tendon healing usually occurs three weeks after repair. The mechanical strength during rupture was used to assess the tendon healing quality four and six weeks after surgery, indicating the maximum tensile strength of the repaired tendon (n = 2 per group at each time). The bones were dissected subperiosteally and transected after the Achilles tendons were dissected from the musculotendinous junction to the calcaneus. The specimens, including the skin, subcutaneous tissue, repaired Achilles tendon, and distal paw, were kept in saline at 4 °C before biomechanical testing. After thawing at room temperature, the distal paw with the insertion of the Achilles tendon was mounted in the upper clamp of the testing machine (Instron 5569, USA). In contrast, the proximal tendon was mounted over the lower clamp.[20,31] The repair site of the Achilles tendon was maintained within the middle of the tested tendon segment. The tensile preload was 0.01 N, and the loading speed was 10 mm/min.

Histological Examination

The specimens were harvested from the musculotendinous junction to the insertion by two longitudinal incisions along the two sides of the Achilles tendon. After the bones were dissected subperiosteally, the specimens, including the skin, subcutis, and repaired tendon, were formalin-fixed and paraffin-embedded.

Two 3 μm slices were longitudinally sectioned from the specimen. After hematoxylin and eosin (H&E) staining, the amount of the NPs was observed at the repair site through a light microscope (40 ×; Olympus BX51, Tokyo, Japan). Then, the degree of adhesions was scored under 100 × magnification based on the grading criteria proposed by Tang et al (Figure 1).[32] The unblinded evaluation was undertaken by two authors, with the final score being a consensus of the two assessments in each region. The degree of adhesions for each group was scored on days 4, 15, 29, and 43 after surgery (n = 2 per group at each time point) to determine whether the anti-adhesive effect of VP-PDA NPs was time-dependent. In addition, the duration of postoperative immobilization after tendon repair in the clinical setting is usually four weeks due to the fibroproliferative phase of the tendon healing process generally lasting 3–4 weeks. We compared adhesion scores among groups four weeks after surgery (n = 8 per group).

Immunohistochemistry

Fibroblast proliferation and fibroblast-to-myofibroblast transition contribute to adhesion formation after tendon repair. The expression of vimentin (a biomarker of fibroblasts) and α-smooth muscle actin (α-SMA; a biomarker of myofibroblasts) in the repaired tendons were evaluated by immunohistochemistry on day 29 (four weeks after surgery) (n = 6 per group). The repaired tendons were harvested from the musculotendinous junction to its insertion. The specimens were

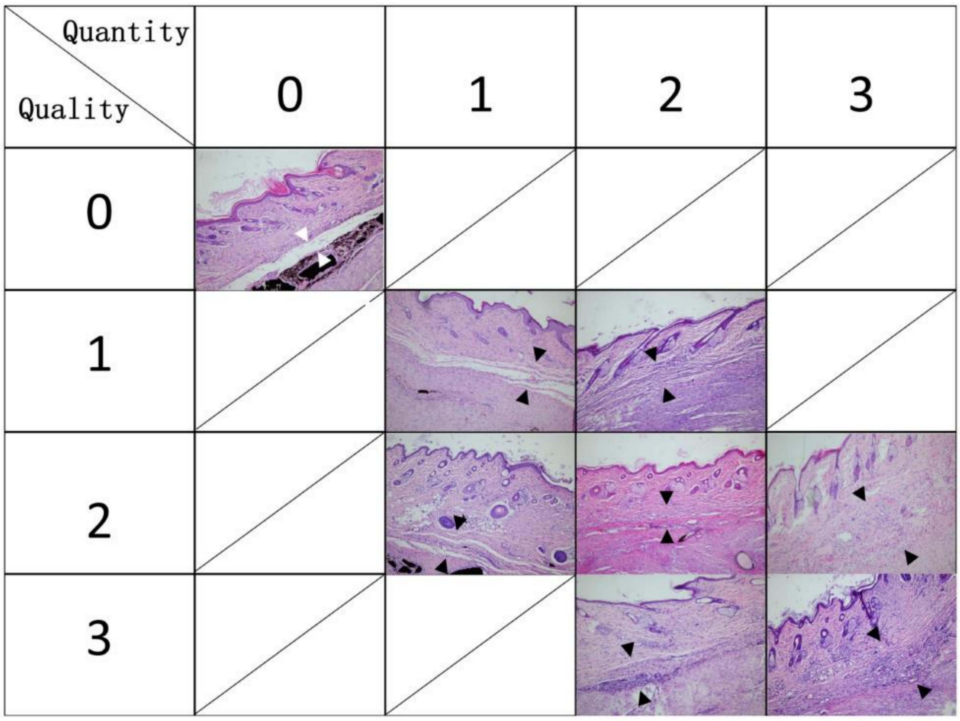

Figure 1 Adhesion formation was scored based on the grading criteria proposed by Tang et al (H&E; 100 ×).[32] Quantitative scores: 0, no adhesion; 1, a few scattered filaments; 2, a large number of filaments; 3, countless filaments. Qualitative scores: 0, no adhesion; 1, regular elongated fine filaments; 2, irregular mixed shortened filaments; 3, dense scar. The adhesion scores = quantitative score + qualitative score. The white arrowheads indicate no adhesion between the tendon surface and subcutaneous tissue; the black arrowheads represent different adhesion formation degrees.

sectioned into 1 μm slices after formalin-fixed and paraffin-embedded. The sections were incubated with rabbit anti-rat antibodies against vimentin (1:200; Cell Signaling Technology, Cat#5741, Beverly, USA) and α-SMA (1: 400; Cell Signaling Technology, Cat# 19245S, Beverly, USA). Then, horseradish peroxidase-conjugated goat anti-rabbit antibodies were utilized as secondary antibodies. 3, 3-diaminobenzidine tetrahydrochloride (DAB) peroxidase substrate solution was used to visualize staining. The expression of vimentin and α-SMA was quantified based on the method proposed by Varghese et al.[33] Five high-power fields were randomly chosen using a light microscope (Olympus BX51, Tokyo, Japan; 400 ×) and captured with cellSens Dimension (Olympus, Tokyo, Japan). The percentages of high positive, positive, and low positive staining were obtained through the ImageJ software (ImageJ 1.51j8; Wayne Rasband, National Institutes of Health, USA) and IHC profiler (https://sourceforge.net/projects/ihcprofiler/). The total score of vimentin and α-SMA was calculated accordingly: Score of expression of vimentin or α-SMA = 3 × percentage of high positive + 2 × percentage of positive + 1× percentage of low positive.

Western Blot

The expression of transforming growth factor-beta 1(TGF-β1) and collagens type I and III in the repaired tendons were detected with Western blot analysis on day 29 (4 weeks after surgery) (n = 6 per group). The tendons were harvested from the musculotendinous junction within the insertion. After being homogenized on ice, the samples were incubated in RIPA lysis buffer for 1 h at 4°C. After centrifugation, the total protein was determined using Enhanced BCA Protein Assay Kit (Sangon Biotech Co. Ltd, Cat# C503051, Shanghai, China). Then, it was separated using sodium dodecylsulphate–polyacrylamide gel electrophoresis (Dake Wei Biological Engineering Co. Ltd, Cat# 8012011, Shenzhen, China), which was then electrotransferred onto polyvinylidene difluoride membranes (GE Healthcare Life Sciences, Cat# 10600023, Freiburg, Germany). The immunoblots were incubated using rabbit anti-rat against TGF-β1 (1:1000; Proteintech, Cat# 21898-1-AP, Chicago, USA), type I collagen (1:1000; Bioss, Cat# bs-10423R, Beijing, China), type III collagen (1:500; Bioss, Cat# bs-0549R, Beijing, China), and anti-GAPDH (1:10,000; Cat#10494-1-AP, Proteintech,

Chicago, USA). After incubation using IRDye 800CW goat anti-rabbit IgG (1:15,000; LI-COR, Cat# 926–32,211, Lincoln, USA), the signals were detected with an infrared dichroic laser scanning imaging system (Odyssey, LI-COR, USA).

Statistical Analysis

Data were analyzed with IBM SPSS Statistics version 25 (IBM Corp., Armonk, NY, USA). The data were represented as mean ± standard error of the mean (SEM). The normality of residuals was tested by the Shapiro–Wilk test. The difference in vimentin and α-SMA between groups was compared using the Kruskal–Wallis test and the Mann–Whitney test with Bonferroni adjustment (0.05/3 = 0.017). The adhesion score difference and failure to load for different times or groups were compared using the two-way analysis of variance (ANOVA) followed by Tukey's test. The difference in adhesion score, TGF-β1, and collagens type I and III among groups four weeks after surgery was compared using the one-way ANOVA followed by Tukey's test. A p-value < 0.05 was considered statistically significant.

Results

Characterization of Nanoparticles

Figure 2A and B show that PDA NPs had a uniform size distribution and an average diameter of 143 nm in the transmission electron microscope (TEM). The size and morphology of VP-PDA NPs did not change significantly after loading verapamil (157 nm). The characteristic peaks associated with verapamil (at 3000 cm^{-1}, 2200 cm^{-1}, 750 cm^{-1}, and 800 cm^{-1}) appeared in Fourier transform infrared spectroscopy (FTIR) spectra of VP-PDA NPs (Figure 2C). This indicated that verapamil was effectively loaded in PDA NPs. Based on the fitted standard curve of ultraviolet (UV) absorbance intensity of solution vs concentration of verapamil, the drug-loading rate and encapsulation efficiency of VP-PDA NPs was 22.7% and 29.3%, respectively (Figures 2D and S1). The loading amount of verapamil in VP-PDA NPs could be determined as 1.135 mg of verapamil in 5 mg VP-PDA NPs (5 mg × 22.7%), depending on the drug-loading rate (Figure S2). The verapamil release test showed that 61.3% of verapamil in VP-PDA NPs was released in vitro for four weeks. Among this, 50% was released in the first 10 days and 11% in the last 18 days (Figure 2E and F).

Before the in vivo application, the biocompatibility of PDA NPs and VP-PDA NPs was evaluated by monitoring the blood biochemistry and H&E staining of vital organs. Table S1 indicates the routine blood biochemical indicators (AST, ALT, CREA, UREA, RBC, Hemoglobin, WBC, and Platelet) without statistical differences between the control and the two administration groups. Additionally, no inflammatory infiltration, edema, or necrosis was observed in the H&E-stained tissue sections of the brain, heart, liver, spleen, lung, and kidney of PDA NPs and VP-PDA NPs groups (Figure S3). Therefore, VP-PDA NPs possessed good biosafety for tendon repair.

Verapamil-Loaded Polydopamine Nanoparticles Enhanced Tendon Healing

Figure 3 illustrates the mechanical strength during tendon rupture (n = 2 per group at each time point). After the normal distribution of the data was tested using the Shapiro–Wilk test (p = 0.863), a two-way ANOVA was performed to assess if there was a difference in the failure to load for different groups or times. We tested the main effects since the interaction test was not significant (F = 2.369, p = 0.174). The main effect was significant (F = 16.355, p = 0.004) for different groups but not for different times (F = 5.655, p = 0.055). Multiple comparisons using Tukey's test indicated a significant increase in average failure to load in the VP-PDA NPs group (89.27 ± 5.09 N) than the PDA NPs (65.52 ± 2.04 N) (p = 0.003) and the control (74.52 ± 4.24 N) (p = 0.029) groups.

Verapamil-Loaded Polydopamine Nanoparticles Decreased Adhesion Scores

Figure 4A demonstrates the change in adhesion scores over time (n = 2 per group at each time point). After the normal distribution of the data was tested using the Shapiro–Wilk test (p = 0.983), a two-way ANOVA determined if there was a difference in adhesion scores for different times or groups. The interaction test between different times and groups was significant (F = 20.707, p<0.001). This indicated that the effect of one independent variable on the dependent variable was dependent on the second variable. The twelve experimental conditions (Control at three days; control at two weeks; control

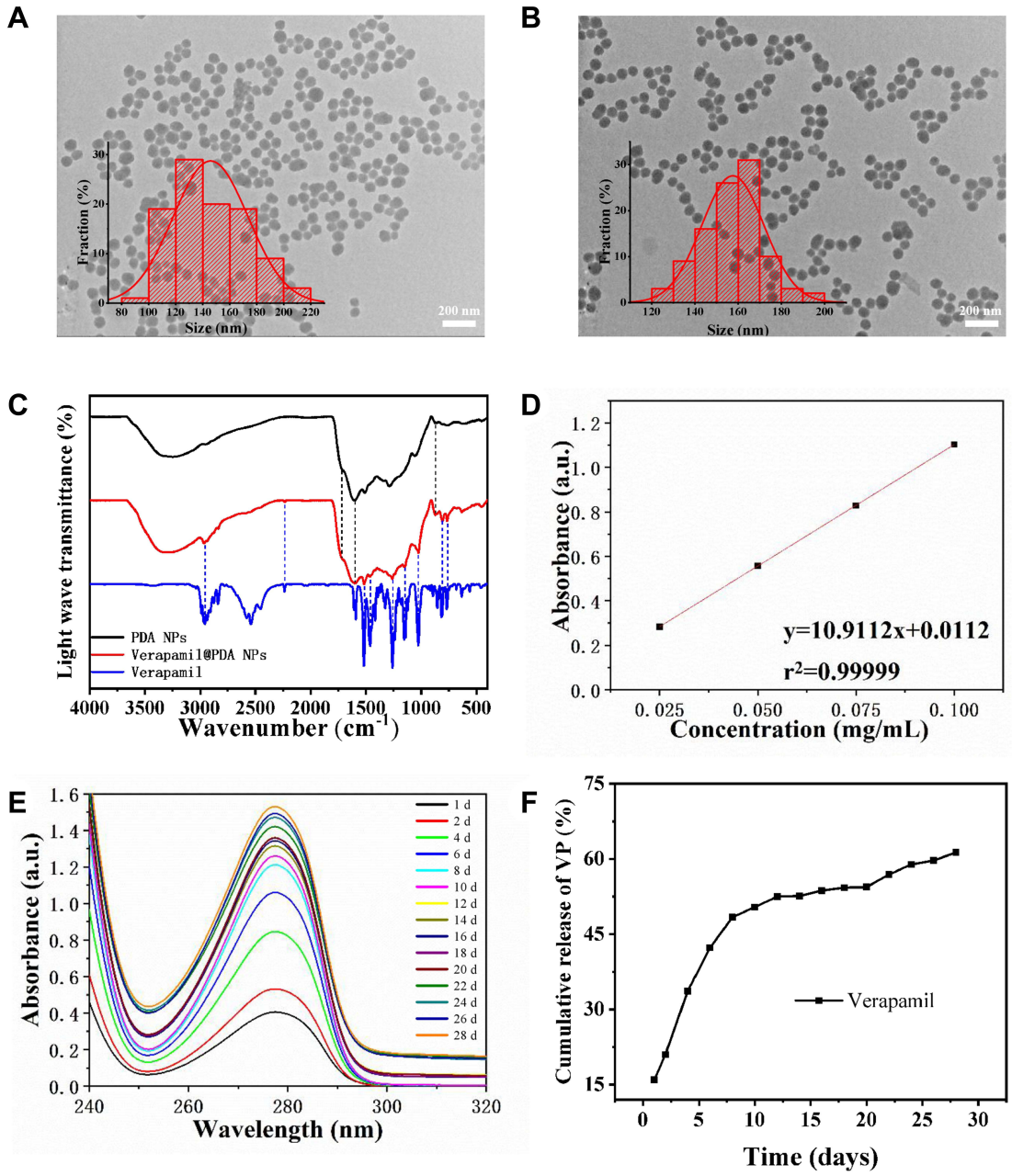

Figure 2 The characterization of polydopamine nanoparticles (PDA NPs) and verapamil-loaded polydopamine nanoparticles (VP-PDA NPs). The transmission electron microscopy (TEM) images of PDA NPs (**A**) and VP-PDA NPs (**B**). The Fourier transform infrared spectroscopy (FTIR) of VP-PDA NPs (**C**). The standard curve represents the UV absorbance value of verapamil solution against verapamil concentration (**D**). The ultraviolet absorbance of released verapamil at a different time point (**E**). The in vitro verapamil release curve of VP-PDA NPs in phosphate buffer saline during four weeks (**F**).

at four weeks, control at six weeks; PDA NPs at three days; PDA NPs at two weeks; PDA NPs at four weeks, PDA NPs at six weeks; VP-PDA NPs at three days; VP-PDA NPs at two weeks; VP-PDA NPs at four weeks, VP-PDA NPs at six weeks) significantly differed while affecting the adhesion scores ($F = 57.268$, $p<0.001$). Tukey's comparisons demonstrated that the significant interaction between different groups and times was because the tendons made significantly fewer adhesion scores in the VP-PDA NPs group at six weeks (3.175 ± 0.08) and four weeks (3.35 ± 0.25) (VP-PDA NPs at six weeks vs VP-PDA NPs at four weeks: $p = 0.994$) than the other groups.

Figure 4B illustrates adhesion scores for each group four weeks after surgery ($n = 8$ per group). After testing the normal distribution using the Shapiro–Wilk test ($p = 0.663$), a one-way ANOVA determined if there was an adhesion score difference for different groups four weeks after surgery. We detected a statistically significant difference in

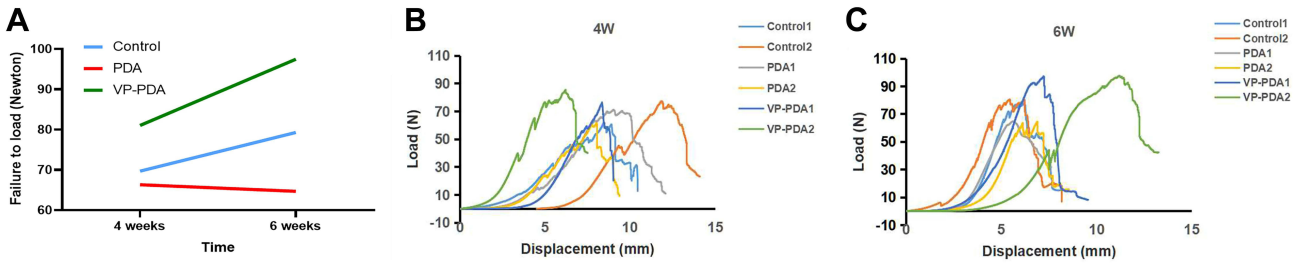

Figure 3 Verapamil-loaded polydopamine nanoparticles enhanced tendon healing. (**A**) The mechanical strength at the time of tendon rupture was used to evaluate the quality of tendon healing. (**B** and **C**) The mechanical strength at the time of tendon rupture at four and six weeks after surgery (n = 2 per group at each time point). **Abbreviations**: PDA NPs, polydopamine nanoparticles; VP-PDA NPs, verapamil-loaded polydopamine nanoparticles.

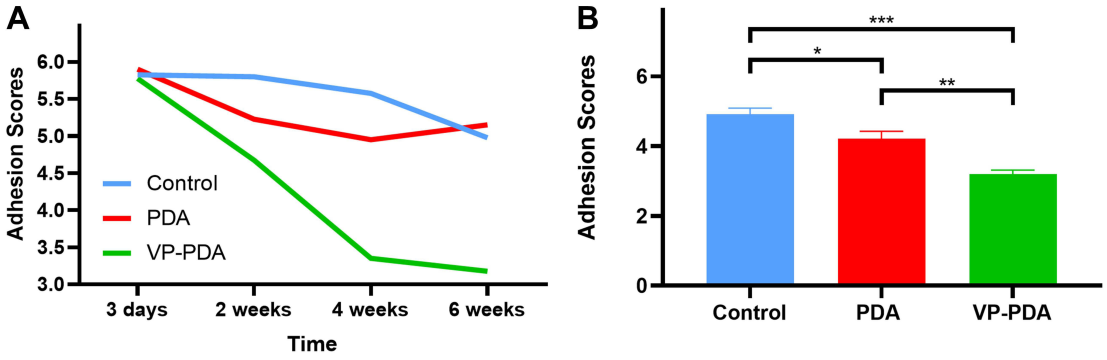

Figure 4 Verapamil-loaded polydopamine nanoparticles decreased adhesion scores after tendon surgery. (**A**) The change in adhesion scores over time (n = 2 per group at each time point). (**B**) Adhesion scores at four weeks after surgery. VP-PDA NPs, verapamil-loaded polydopamine nanoparticles. PDA NPs, polydopamine nanoparticles. The bars represent mean ± SEM (n = 8 per group). *p<0.05; **p<0.01; ***p<0.001.

adhesion scores among the groups (F = 23.70, p<0.001). Results from Tukey's comparisons indicated that the adhesion score was significantly decreased in the VP-PDA NPs group (3.19 ± 0.12), followed by the PDA NPs group (4.21 ± 0.22) and then the control group (4.91 ± 0.18) (VP-PDA NPs vs Control: p<0.001; VP-PDA NPs vs PDA NPs: p = 0.002; PDA NPs vs Control: p = 0.028) (Figure 4B).

Nanoparticles Decreased Over Time

Figure 5 illustrates the histology of repaired tendons. No skin ulcers or infections were observed in all the rats. The amount of VP-PDA NPs and PDA NPs decreased over time (n = 2 per group at each time point). Moreover, a space between the tendon surface and surrounding tissue was observed in the VP-PDA NPs group four weeks after surgery.

Verapamil-Loaded Polydopamine Nanoparticles Inhibited Fibroblast Proliferation

Figure 6A and B illustrate the vimentin expression (a biomarker of fibroblasts) in the repaired tendons (n = 6 per group). A statistically significant difference was observed in the vimentin expression scores among groups ($\chi^2 = 9.93$; p = 0.007). The Mann–Whitney test using Bonferroni adjustment (0.05/3 = 0.017) observed that the difference lied in between the VP-PDA NPs (44.91 ± 3.02) and the control (63.55 ± 3.55) (p = 0.010) groups and between the VP-PDA NPs and the PDA NPs (57.07 ± 2.43) (p = 0.010) groups. However, there was no significant difference between the control and the PDA NPs (p = 0.150) groups.

Verapamil-Loaded Polydopamine Nanoparticles Inhibited Fibroblast-to-Myofibroblast Transition

Figure 6A and C illustrate the expression of α-SMA (a biomarker of myofibroblasts) in the repaired tendons (n = 6 per group). A statistically significant difference was observed in α-SMA among groups ($\chi^2 = 8.19$; p = 0.017; n = 6 per group). The Mann–

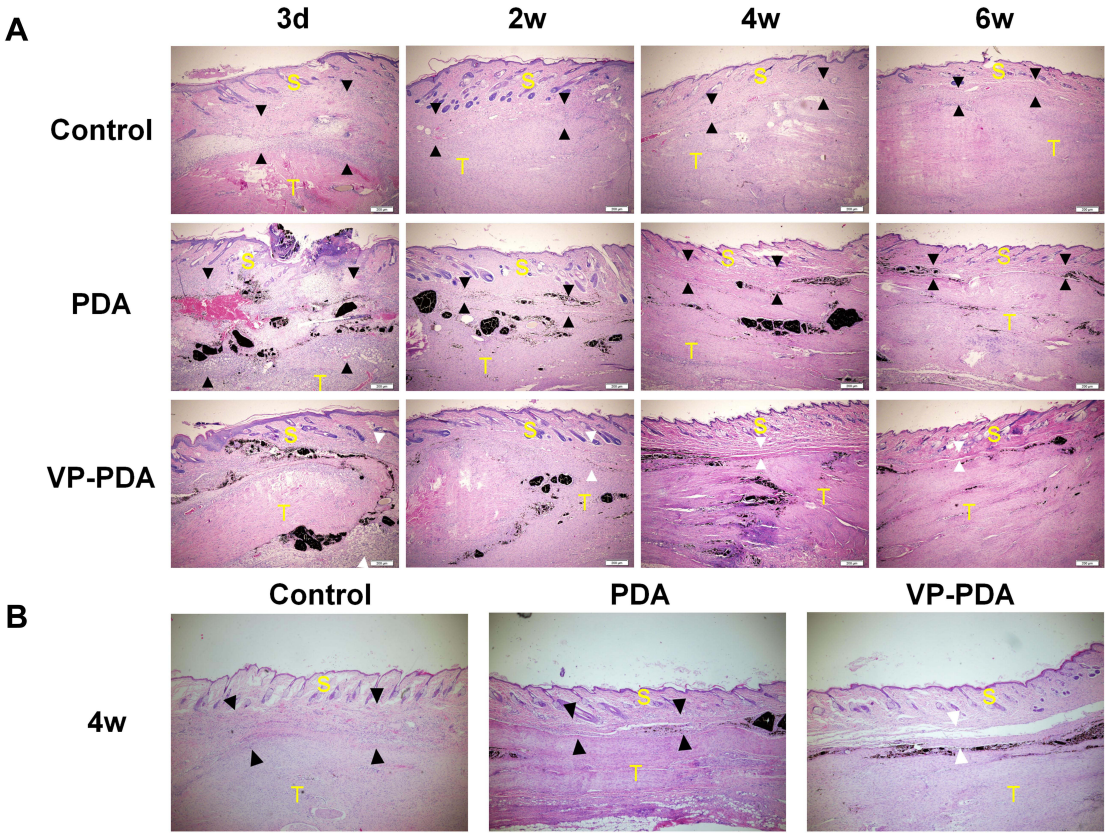

Figure 5 Nanoparticles decreased over time in vivo (H&E; 40 ×). (**A**) The change in the number of nanoparticles within the repair site over time. (**B**) A space exists between the tendon surface and surrounding tissue within the VP-PDA NPs group four weeks after surgery. PDA NPs, polydopamine nanoparticles. VP-PDA NPs, verapamil-loaded polydopamine nanoparticles. S indicates the skin and subcutaneous tissue, and T denotes the tendon. The black arrowheads indicate adhesion formation, and the white arrowheads indicate space.

Whitney test using Bonferroni adjustment (0.05/3 = 0.017) identified that the difference lied in between the VP-PDA NPs (23.88 ± 2.40) and the PDA NPs (37.56 ± 2.75) (p = 0.010) groups. However, no significant difference was observed between the VP-PDA NPs and the control (47.08 ± 7.71) (p = 0.025) groups and between the PDA NPs and the control (p = 0.337) groups.

Verapamil-Loaded Polydopamine Nanoparticles Inhibited the Expression of Transforming Growth Factor-Beta 1

Figure 7A illustrates the expression of TGF-β1 in the repaired tendons at four weeks after surgery (n = 6 per group). A significant difference was observed in TGF-β1 across the three groups (F = 14.332; p<0.001). The post hoc Tukey's test found that the lowest expression of TGF-β1 was within the VP-PDA NPs group (0.425 ± 0.08), followed by the PDA NPs group (0.822 ± 0.12) and then the control group (1.23 ± 0.11).

Verapamil-Loaded Polydopamine Nanoparticles Decreased the Content of Collagens

Figure 7B and C illustrate the expression of collagens type I and III in the repaired tendons four weeks after surgery (n = 6 per group). The average expression of collagens was different across groups (type I: F = 18.164; p<0.001; type III: F = 24.491; p<0.001). Post hoc Tukey's multiple comparisons observed that the collagen expression was the lowest in the VP-PDA NPs group (type I: 0.373 ± 0.09; type III: 0.158 ± 0.03), followed by the PDA NPs group (type I: 0.737 ± 0.09; type III: 0.322 ± 0.03) and then the control group (type I: 1.143 ± 0.09; type III: 0.482 ± 0.04).

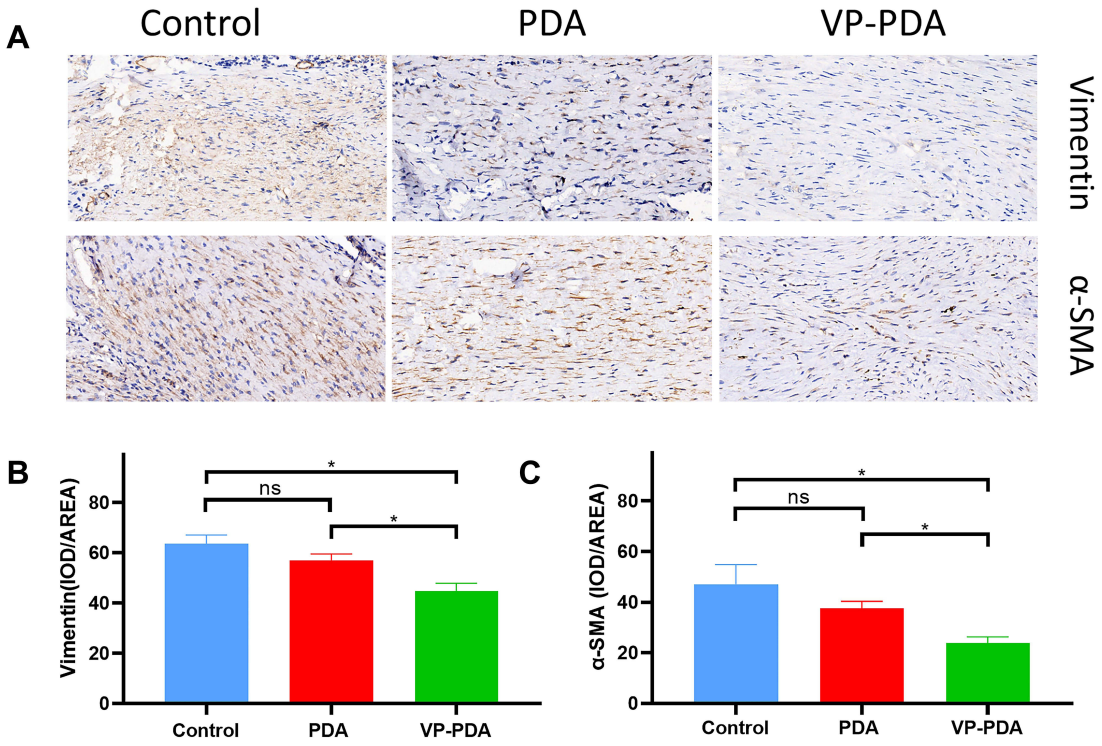

Figure 6 Verapamil-loaded polydopamine nanoparticles reduced the expression of vimentin and α-smooth muscle actin (α-SMA) in the repaired tendons at four weeks after surgery. (**A**) The expression of vimentin and α-SMA was detected using immunohistochemistry. (**B** and **C**) The expression scores in vimentin and α-SMA. PDA NPs, polydopamine nanoparticles. VP-PDA NPs, verapamil-loaded polydopamine nanoparticles. The bars represent mean ± SEM (n = 6 per group) *p<0.05; ns, not significant.

Discussion

The goal of tendon repair is to achieve tendon healing and restore gliding for functional success.[4] The present study demonstrated the anti-adhesive effects of VP-PDA NPs on adhesion formation after tendon repair. Simultaneously, biomechanical data indicated that the tendon healing quality by VP-PDA NPs is better than that in the control and the PDA groups. Histological examination revealed that VP-PDA NPs significantly reduced adhesion scores. However, no significant difference was observed between the PDA NPs and the control groups, indicating the anti-adhesive effect of VP-PDA NPs due to verapamil.

After tendon injury and repair, the healing scheme includes an inflammatory phase of 48–72 hours, a fibroblastic proliferation phase lasting 3–4 weeks, and a remodeling period.[4] Upon tendon injury, both inflammatory response and oxidative stress become intense at the injury site within 24 hours.[34,35] Inflammatory cells release various proinflammatory cytokines, including TGF-β1, tumor necrosis factor α, interleukin 1β, etc. TGF-β1 has been associated with excessive scar formation after tendon injury.[1,36] They potently activate fibroblasts and can induce fibrosis in vivo.[37] In addition, TGF-β1 activates and differentiates fibroblasts from myofibroblasts. Myofibroblasts specifically express α-SMA, producing a more collagenous extracellular matrix than fibroblasts.[38–40] TGF-β1 is critical in the pathogenesis of adhesion formation after tendon injury. However, complete TGF-β1 blockage affects tendon healing.[1] In the current study, VP-PDA NPs inhibited expression of TGF-β1, fibroblast proliferation, and fibroblast-to-myofibroblast transition other than decreasing the content of type I and III collagens. In vitro study by Roth et al has demonstrated that calcium channel blockers reduce collagen deposition by inhibiting the expression of collagens type I and III. Moreover, they increase the proteolytic activity of collagenase type III.[29] Therefore, the results from our study are consistent with previous reports.[22–29] VP-PDA NPs significantly reduced the content of collagens type I and III after tendon injuries. It was postulated that VP-PDA NPs could produce anti-adhesive effects by inhibiting TGF-β1 expression, thereby inhibiting fibroblast proliferation and activation. However, further investigation is required to validate the hypothesis.

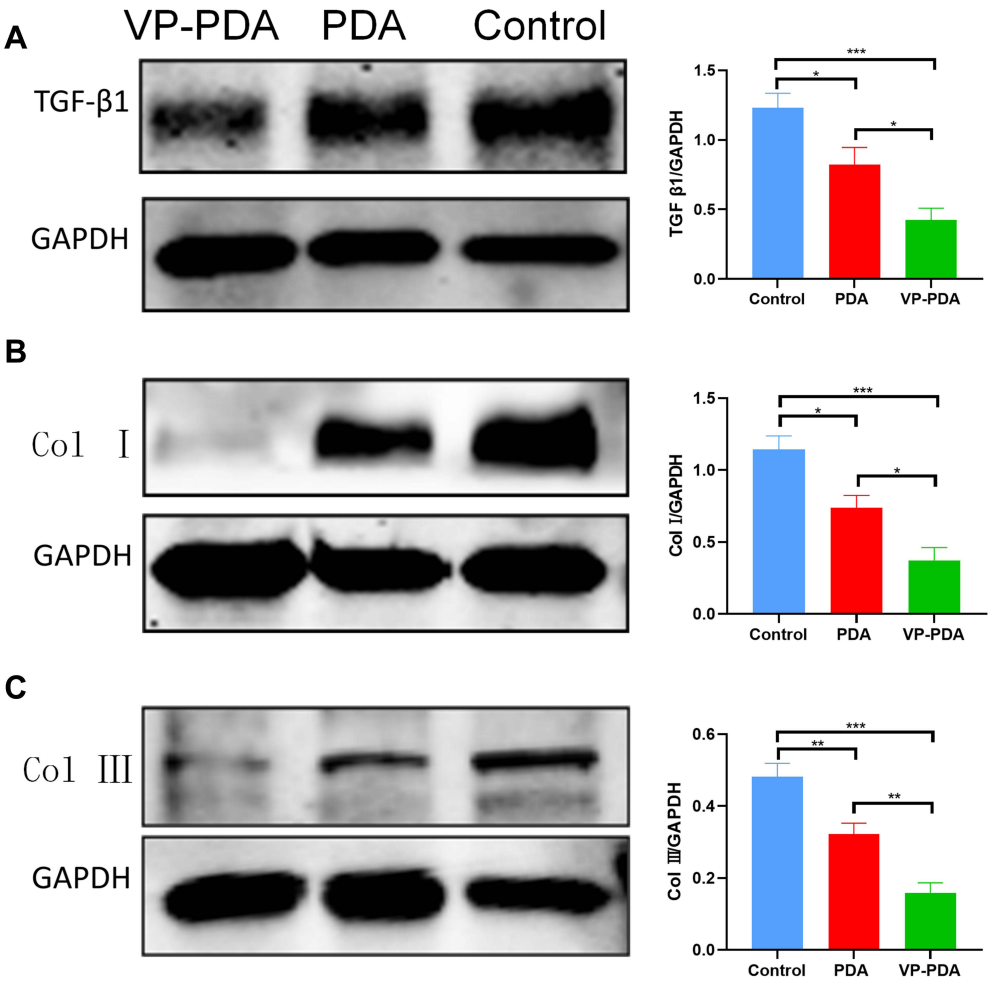

Figure 7 Verapamil-loaded polydopamine nanoparticles decreased the expression of (**A**) TGF-β1, (**B**) collagen type I, and (**C**) collagen type III in the repaired tendons at four weeks after surgery. PDA NPs, polydopamine nanoparticles. VP-PDA NPs, verapamil-loaded polydopamine nanoparticles. The bars represent mean ± SEM (n = 6 per group). *p<0.05; **p<0.01; ***p<0.001.

Several studies have evaluated the therapeutic effect of verapamil on scar formation in patients having keloids and hypertrophic scars, depending on the anti-fibrotic effects of topical verapamil.[22,24,26] For example, Abou-Taleb et al reported that intralesional injection of verapamil had excellent improvement in 53.5% (out of 43) patients with keloids.[24] However, previous studies on the anti-fibrotic effects of topical verapamil have focused on fibroproliferative skin lesions. Moreover, few studies have investigated the role of topical verapamil in adhesion formation pathogenesis after tendon repair.

The anti-fibrotic effects of verapamil can be achieved by improving the durability of verapamil for clinical efficacy. Many substances, such as 5-fluorouracil, alginate, or corticosteroids, fail to persist long enough to attain anti-adhesive effects.[32] Oral administration of verapamil may lower systemic blood pressure. Its local injection is also not practical for patients with tendon injuries because the anti-fibrotic effects need a more extended treatment period. Polydopamine (PDA) is a melanin-like polymer possessing excellent biocompatibility.[41] Nanoparticles have biodegradability and controlled release ability, and these advantages have been used for drug delivery or gene transfer.[20] Nanoparticles can persistently release their contents over a prolonged time.[20] Our in vitro assay revealed that the release of verapamil persists for at least four weeks after the fibroblastic phase.

However, the appropriate dosage of verapamil in VP-PDA NPs needs further investigation to prevent adhesion formation after tendon injury. In the study, 5 mg VP-PDA NPs had 1.135 mg verapamil hydrochloride. The in vitro release test revealed that the cumulative release amount of verapamil was 0.696 mg in four weeks, comparable to Rha

et al.[25] In their study, 0.58 mg verapamil was released from the silicone gel sheet with 2.5 mg verapamil in four weeks. Their results in a rabbit ear wound model indicated that 0.58 mg verapamil significantly reduced the mean scar elevation index, fibroblast counts, and capillary counts.[24]

From a clinical perspective, VP-PDA NPs can reduce adhesion formation after tendon injury. However, certain limitations are worth noting. First, the rat model of Achilles tendon laceration and repair in the study is an extrasynovial flexor injury. It is unknown whether VP-PDA NPs reduce the adhesion formation of intrasynovial tendons like the digital flexor tendons of the hand. Second, whether the anti-adhesive effects of verapamil correlate with drug dosage and the timing of releasing the drug is unknown. Therefore, future studies should evaluate optimal dosage, release timing, and whether VP-PDA NPs are suitable for intrasynovial tendon injury. In addition, PDA NPs are polymers with near-infrared absorbing ability. Hence, their inherent photothermal properties could be beneficial for promoting tendon healing and reducing tendon adhesion.

Conclusion

A novel formulation of verapamil, VP-PDA NPs, was developed for reducing adhesion formation after tendon injury. In rat Achilles injury model, VP-PDA NPs reduced adhesion formation and also enhanced tendon healing. Therefore, VP-PDA NPs would have direct translation implications as topical verapamil is well tolerated, and intralesional injection of verapamil is currently being used in clinical settings.

Acknowledgments

We would like to appreciate the technical help from the Central Laboratory and Department of Pathology, the First Hospital (Section 2) of Jilin University. The preparation and characterization of PDA and VP-PDA NPs were performed by State Key Laboratory of Supramolecular Structure and Materials, College of Chemistry, Jilin University. We would like to thank MogoEdit for its English editing during the preparation of this manuscript.

Disclosure

The authors report no conflicts of interest in this work.

References

1. Titan AL, Foster DS, Chang J, et al. Flexor tendon: development, healing, adhesion formation, and contributing growth factors. *Plast Reconstr Surg*. 2019;144:639e–647e. doi:10.1097/PRS.0000000000006048
2. Nichols AEC, Best KT, Loiselle AE. The cellular basis of fibrotic tendon healing: challenges and opportunities. *Transl Res*. 2019;209:156–168. doi:10.1016/j.trsl.2019.02.002
3. Legrand A, Kaufman Y, Long C, et al. Molecular biology of flexor tendon healing in relation to reduction of tendon adhesions. *J Hand Surg Am*. 2017;42:722–726. doi:10.1016/j.jhsa.2017.06.013
4. Sammer DM, Chung KC. Advances in the healing of flexor tendon injuries. *Wound Repair Regen*. 2014;22(Suppl 1):25–29. doi:10.1111/wrr.12161
5. Zhou H, Lu H. Advances in the development of anti-adhesive biomaterials for tendon repair treatment. *Tissue Eng Regen Med*. 2021;18:1–14. doi:10.1007/s13770-020-00300-5
6. Moran SL, Ryan CK, Orlando GS, et al. Effects of 5-fluorouracil on flexor tendon repair. *J Hand Surg Am*. 2000;25:242–251. doi:10.1053/jhsu.2000.jhsu25a0242
7. Zhao C, Zobitz ME, Sun YL, et al. Surface treatment with 5-fluorouracil after flexor tendon repair in a canine in vivo model. *J Bone Joint Surg Am*. 2009;91:2673–2682. doi:10.2106/JBJS.H.01695
8. de Wit T, de Putter D, Tra WM, et al. Auto-crosslinked hyaluronic acid gel accelerates healing of rabbit flexor tendons in vivo. *J Orthop Res*. 2009;27:408–415. doi:10.1002/jor.20730
9. Tan V, Nourbakhsh A, Capo J, et al. Effects of nonsteroidal anti-inflammatory drugs on flexor tendon adhesion. *J Hand Surg Am*. 2010;35:941–947. doi:10.1016/j.jhsa.2010.02.033
10. Zhao C, Ozasa Y, Shimura H, et al. Effects of lubricant and autologous bone marrow stromal cell augmentation on immobilized flexor tendon repairs. *J Orthop Res*. 2016;34:154–160. doi:10.1002/jor.22980
11. Orner CA, Geary MB, Hammert WC, et al. Low-dose and short-duration matrix metalloproteinase 9 inhibition does not affect adhesion formation during murine flexor tendon healing. *Plast Reconstr Surg*. 2016;137:545e–553e. doi:10.1097/01.prs.0000475823.01907.53
12. Fatemi MJ, Shirani S, Sobhani R, et al. Prevention of peritendinous adhesion formation after the flexor tendon surgery in rabbits: a comparative study between use of local interferon-alpha, interferon-beta, and 5-fluorouracil. *Ann Plast Surg*. 2018;80:171–175. doi:10.1097/SAP.0000000000001169
13. Zhao C, Sun YL, Kirk RL, et al. Effects of a lubricin-containing compound on the results of flexor tendon repair in a canine model in vivo. *J Bone Joint Surg Am*. 2010;92:1453–1461. doi:10.2106/JBJS.I.00765

14. Hung LK, Fu SC, Lee YW, et al. Local vitamin-C injection reduced tendon adhesion in a chicken model of flexor digitorum profundus tendon injury. *J Bone Joint Surg Am*. 2013;95:e41. doi:10.2106/JBJS.K.00988
15. Tang JB, Cao Y, Zhu B, et al. Adeno-associated virus-2-mediated bFGF gene transfer to digital flexor tendons significantly increases healing strength. An in vivo study. *J Bone Joint Surg Am*. 2008;90:1078–1089. doi:10.2106/JBJS.F.01188
16. Chen CH, Zhou YL, Wu YF, et al. Effectiveness of microRNA in down-regulation of TGF-beta gene expression in digital flexor tendons of chickens: in vitro and in vivo study. *J Hand Surg Am*. 2009;34:1777–1784. doi:10.1016/j.jhsa.2009.07.015
17. Wu YF, Mao WF, Zhou YL, et al. Adeno-associated virus-2-mediated TGF-beta1 microRNA transfection inhibits adhesion formation after digital flexor tendon injury. *Gene Ther*. 2016;23:167–175. doi:10.1038/gt.2015.97
18. Weng CJ, Liao CT, Hsu MY, et al. Simvastatin-loaded nanofibrous membrane efficiency on the repair of achilles tendons. *Int J Nanomedicine*. 2022;17:1171–1184. doi:10.2147/IJN.S353066
19. Hadda Z, Hélène VDB, Tom P, et al. Preliminary in vivo study of biodegradable PLA-PEU-PLA anti-adhesion membranes in a rat Achilles tendon model of peritendinous adhesions. *Biomater Sci*. 2022;10:1776–1786. doi:10.1039/D1BM01150B
20. Zhou YL, Zhang LZ, Zhao WX, et al. Nanoparticle-mediated delivery of TGF-β1 miRNA plasmid for preventing flexor tendon adhesion formation. *Biomaterials*. 2013;34:8269–8278. doi:10.1016/j.biomaterials.2013.07.072
21. Weng CJ, Lee D, Ho J, et al. Doxycycline-embedded nanofibrous membranes help promote healing of tendon rupture. *Int J Nanomedicine*. 2020;15:125–136. doi:10.2147/IJN.S217697
22. Lee RC, Doong H, Jellema AF. The response of burn scars to intralesional verapamil. Report of five cases. *Arch Surg*. 1994;129:107–111. doi:10.1001/archsurg.1994.01420250119015
23. Choi J, Han YN, Rha EY, et al. Verapamil-containing silicone gel reduces scar hypertrophy. *Int Wound J*. 2021;18:647–656. doi:10.1111/iwj.13566
24. Abou-Taleb DAE, Badary DM. Intralesional verapamil in the treatment of keloids: a clinical, histopathological, and immunohistochemical study. *J Cosmet Dermatol*. 2021;20:267–273. doi:10.1111/jocd.13476
25. Rha EY, Kim YH, Kim TJ, et al. Topical application of a silicone gel sheet with verapamil microparticles in a rabbit model of hypertrophic scar. *Plast Reconstr Surg*. 2016;137:144–151. doi:10.1097/PRS.0000000000001889
26. Boggio RF, Boggio LF, Galvão BL, et al. Topical verapamil as a scar modulator. *Aesthetic Plast Surg*. 2014;38:968–975. doi:10.1007/s00266-014-0400-9
27. Boggio RF, Freitas VM, Cassiola FM, et al. Effect of a calcium-channel blocker (verapamil) on the morphology, cytoskeleton and collagenase activity of human skin fibroblasts. *Burns*. 2011;37:616–625. doi:10.1016/j.burns.2010.07.012
28. Zeng MQ, Xiao W, Yang K, et al. Verapamil inhibits ureteral scar formation by regulating CaMK II-mediated Smad pathway. *Chem Biol Interact*. 2021;346:109570. doi:10.1016/j.cbi.2021.109570
29. Roth M, Eichel Berg O, Kohler E, et al. Ca2+ channel blockers modulate metabolism of collagens within the extracellular matrix. *Proc Natl Acad Sci USA*. 1996;93:5478–5482. doi:10.1073/pnas.93.11.5478
30. Wong JK, Lui YH, Kapacee Z, et al. The cellular biology of flexor tendon adhesion formation: an old problem in a new paradigm. *Am J Pathol*. 2009;175:1938–1951. doi:10.2353/ajpath.2009.090380
31. Zhou YC, Xie SS, Tang YF, et al. Effect of book-shaped acellular tendon scaffold with bone marrow mesenchymal stem cells sheets on bone-tendon interface healing. *J Orthop Translat*. 2020;26:162–170. doi:10.1016/j.jot.2020.02.013
32. Tang JB, Ishii S, Usui M, et al. Dorsal and circumferential sheath reconstructions for flexor sheath defect with concomitant bony injury. *J Hand Surg Am*. 1994;19:61–69. doi:10.1016/0363-5023(94)90225-9
33. Varghese F, Bukhari AB, Malhotra R, et al. IHC profiler: an open source plugin for the quantitative evaluation and automated scoring of immunohistochemistry images of human tissue samples. *PLoS One*. 2014;9:e96801. doi:10.1371/journal.pone.0096801
34. Li PF, Zhou HY, Tu T, et al. Dynamic exacerbation in inflammation and oxidative stress during the formation of peritendinous adhesion resulted from acute tendon injury. *J Orthop Surg Res*. 2021;16:293. doi:10.1186/s13018-021-02445-y
35. Xu HT, Lee CW, Li MY, et al. The shift in macrophages polarisation after tendon injury: a systematic review. *J Orthop Translat*. 2019;21:24–34. doi:10.1016/j.jot.2019.11.009
36. Zhang AY, Pham H, Ho F, et al. Inhibition of TGF-beta-induced collagen production in rabbit flexor tendons. *J Hand Surg Am*. 2004;29:230–235. doi:10.1016/j.jhsa.2003.11.005
37. Reich N, Tomcik M, Zerr P, et al. Jun N-terminal kinase as potential molecular target for prevention and treatment of dermal fibrosis. *Ann Rheum Dis*. 2012;71:737–745. doi:10.1136/annrheumdis-2011-200412
38. Lebonvallet N, Laverdet B, Misery L, et al. New insights into the roles of myofibroblasts and innervation during skin healing and innovative therapies to improve scar innervation. *Exp Dermatol*. 2018;27:950–958. doi:10.1111/exd.13681
39. Hinz B, Phan SH, Thannickal VJ, et al. Recent developments in myofibroblast biology: paradigms for connective tissue remodeling. *Am J Pathol*. 2012;180:1340–1355. doi:10.1016/j.ajpath.2012.02.004
40. Hinz B, Phan SH, Thannickal VJ, et al. The myofibroblast: one function, multiple origins. *Am J Pathol*. 2007;170:1807–1816. doi:10.2353/ajpath.2007.070112
41. Yazdi MK, Zare M, Khodadadi A, et al. Polydopamine biomaterials for skin regeneration. *Biomater Sci Eng*. 2022;8(6):2196–2219. doi:10.1021/acsbiomaterials.1c01436